


Influence of pre-strain and bake hardening on the static and fatigue strength of a DP600 steel sheet

Andrea Kusch¹ | Daniele Crivelli¹ | Luca Diviani¹ | Matteo Dotta¹ |
Simone Salamina¹ | Filippo Berto² 

¹Department of Innovative Technologies, University of Applied Sciences and Arts of Southern Switzerland (SUPSI), Lugano, Switzerland

²Department of Chemical Engineering Materials Environment, Sapienza University of Rome, Rome, Italy

Correspondence

Simone Salamina, Department of Innovative Technologies, University of Applied Sciences and Arts of Southern Switzerland (SUPSI), Lugano, Switzerland.

Email: simone.salamina@supsi.ch

Funding information

Innosuisse - Swiss Innovation Agency, Grant/Award Number: 55512.1 IP-ENG

Abstract

The influence of pre-strain on the tensile and fatigue properties of a dual phase DP600 steel was studied. The material was pre-strained by uni-axial tension in rolling and transverse direction. Thereafter, specimens were cut from the deformed plates in parallel or orthogonal to pre-strain direction. It was found that pre-strain increases yield and tensile strength. Results suggested that strain path change primarily affects the elastic-plastic transition during early stage of reloading. Pre-strained specimens showed an increase in high cycle regimes as a consequence of yield strength increment, irrespective of imposed pre-straining direction. A modified stress life equation that accounts for pre-strain was proposed and showed good agreement with experimental data. Bake hardening enhanced both tensile and high cycle fatigue resistance. Walker equation was successfully fitted to account for tensile mean stress. In low cycle fatigue, negligible influence of pre-strain was observed due to cyclic softening and residual stress relaxation.

KEYWORDS

bake hardening, DP steels, HCF, LCF, mean stress, pre-strain

Highlights

- A DP600 steel sheet is characterized under different pre-strain conditions and after baking.
- Experiments indicate that pre-strain and bake hardening are beneficial in HCF.
- Modified Basquin equations to account for the effect of pre-strain and bake hardening are proposed.
- Walker mean stress correction shows good agreement with experimental data.

This is an open access article under the terms of the [Creative Commons Attribution-NonCommercial](https://creativecommons.org/licenses/by-nc/4.0/) License, which permits use, distribution and reproduction in any medium, provided the original work is properly cited and is not used for commercial purposes.

© 2023 The Authors. *Fatigue & Fracture of Engineering Materials & Structures* published by John Wiley & Sons Ltd.

1 | INTRODUCTION

Fatigue is one of the most critical aspects to be considered when designing new components, but it is often very difficult to predict the life expectancy of structures subjected to cyclic loads. Among the other fundamental variables influencing the strength of the material, the manufacturing processes can play a significant role.

Sheet metal forming is a commonly used manufacturing method in the automotive industry. This process involves high deformation of the steel sheets. Moreover, components may undergo baking after painting, which further alters the mechanical properties. Therefore, fatigue assessment of components may be even more challenging after these procedures.

During the cold forming process, the material is pressed in stamps to obtain the desired shape. This operation results in three main effects on the material: straining, thinning, and rising of residual stresses. Thinning is easily obtained through finite elements analysis or direct measurements on the wheel, and it is only a geometrical aspect, because it does not involve material properties. Residual stresses at the end of the forming process can also be evaluated using finite elements analysis, and they are treated as mean stresses for fatigue assessment.¹ Consequently, a precise mean stress model is needed to assess fatigue strength in the presence of residual stresses. Additionally, straining directly influences material properties due to hardening and reduced ductility. Thus, fatigue assessment considering the effect of prior deformation is more accurate.^{2,3}

2 | OVERVIEW OF RECENT DEVELOPMENTS

2.1 | Dual phase steels—properties and microstructure

Automotive is the major field of application of dual phase steels, where, thanks to their high strength and formability, they contribute to limiting the mass of the vehicles in order to reduce fuel consumption and emissions. Because of their application, the assessment of their fatigue resistance is of paramount importance. Furthermore, the effects of the manufacturing processes on the properties of DP steels are a hot topic in the scientific literature.

DP steels are produced by intercritical annealing of low carbon, low alloy steels.⁴ The controlled cooling from the austenite + ferrite temperature range results in the transformation of austenite in martensite. Continuous yielding and low yield to tensile strength ratio are a consequence of the high density of mobile dislocations in

ferrite created during austenite-martensite transformation.^{5,6} The behavior of DP steels is strongly related with their composite microstructure, consisting in hard martensite particles dispersed in a soft ferrite matrix, because of the heterogeneous strain distribution in the two phases.^{7–9} In general, tensile strength is improved with increasing martensite content, while its dispersion determines ductility.^{6,10–13} For the same volume fraction of martensite, a finely dispersed microstructure shows the best combination of strength and ductility.^{14–16}

The fatigue properties depend on the combination of both strength and ductility. HCF is mostly affected by the former, while the latter is more influential for LCF regimes. Thus, higher martensite contents result in enhanced long fatigue lives,^{13,15–17} whereas at shorter lives, the interaction between the phases becomes more important. In particular, for low martensite content, only ferrite deforms and cyclic hardening is observed, and for higher percentage of hard phase, the material exhibits cyclic softening due to internal stress relief.^{12,18,19} At the same time, martensite particles hinder crack propagation, so a uniform distribution is preferred for fatigue resistance.^{16,20}

2.2 | Influence of pre-strain

Over the last decades, various researchers studied the effect of prior deformation on the mechanical properties of dual phase steels. Pre-strain is known to increase yield and tensile strength due to work hardening and reduce ductility.^{21–25} Different straining paths, however, result in distinct material response.^{26–29} In particular, while a sharp yield point is expected, tensile tests in a direction different to that of pre-strain result in lower elastic limit increment and rounding of the flow curve.^{26,28,30} Furthermore, changes in elastic modulus after pre-strain have been reported in literature.^{29,31,32}

For fatigue strength, literature is more controversial. In general, an improvement in HCF resistance is expected after pre-strain as a consequence of higher yield strength, while a detrimental effect of prior deformation may be observed for LCF as some capacity of the material to plastically deform is lost. However, other researchers observed a beneficial effect of pre-strain even for LCF regimes.^{33–35} Friedriksson et al^{21,22} performed strain controlled fatigue tests on DP400 and DP600 sheets with different treatments before testing, such as uni-axial, equi-biaxial, or plane strain deformation and aging. Monotonic properties improved compared to the as-received condition, but fatigue life was not very sensitive to pre-straining. Gustavsson et al^{33,34,36} tested the effect of prestrain on the fatigue properties of DP440 and DP400 steels and found a

weak positive influence on LCF. Le et al^{24,37} tested fatigue performance of a DP600 sheet steel after uni-axial and plane strain pre-strain. While uniaxially pre-strained specimens exhibited higher fatigue strength compared to as-received condition in the long life domain and lower fatigue strength for life less than 10^3 cycles, plane strain pre-strain did improve fatigue strength throughout its lifetime. Based upon these results, the same authors³⁸ also proposed a modified strain-life equation to consider the effect of different pre-strain paths. Das et al^{39–42} studied the effect of pre-strain on the tensile, HCF, LCF, and notch fatigue performance of a DP600 steel sheet. Testing was performed in both parallel and orthogonal direction to pre-strain. An increase in long lives was observed, testing orthogonal to pre-strain resulted in better improvement. Short lives decreased after strain path change, while no significant difference in LCF was observed after pre-strain in the same direction to testing. Minor positive effect on notch fatigue was explained due to higher stress concentration caused by increased yield strength, which nullified the beneficial effect of pre-strain on HCF. The same research group also studied the influence of uni-axial and bi-axial pre-strain on a DP590 steel.^{43–45} Bi-axial pre-strain was found to increase strength and reduce ductility more than uni-axial pre-strain for equivalent plastic strain. This resulted in significant improvement of long life and reduction of short lives.

Louge et al^{46,47} proposed a new method to assess the effect of load history on the HCF by means of self-heating measurements under cyclic loading. This approach showed good agreement with experimental results on a high strength low alloy steel sheet.

Paul⁴⁸ recently published a comprehensive literature review on the impact of forming strain on dual phase steels. Nevertheless, despite strong efforts to understand the influence of pre-strain on fatigue strength of dual phase steels, literature still lacks a comprehensive study that takes into account various levels of deformation for different straining paths.

2.3 | Bake hardening

Although DP steels do not undergo aging at room temperature, after the paint baking process, an increase in yield strength is noticed.⁴ This bake hardening (BH) effect can be explained by three different mechanisms: diffusion of

interstitial atoms toward mobile dislocation (Cottrell atmospheres), formation of precipitates and carbides in ferrite, and tempering of martensite.^{49–53} Bake hardening, however, has a limited effect on ultimate strength and ductility,²³ so no differences in LCF regimes are observed after this treatment,^{21,35,54} while an improvement in HCF lives is expected,⁵⁵ as a consequence of higher yield strength. Work and bake hardening interaction have been studied, and a decreasing effect of BH with pre-strain was observed.^{49,56,57}

2.4 | Mean stress correction

Various models are proposed in the literature to account for mean stresses. Among the most common mean stress correction approaches are from Gerber, Goodman, Soderberg, Morrow, Smith-Watson-Topper (SWT), and Walker.⁵⁸ The Walker model, a modification of the SWT model, thanks to his adjustable parameter, is more versatile.⁵⁹ Despite the relevance of mean stress in dual phase steels applications, little research is found in literature about this topic. Giri and Bhattacharjee⁶⁰ documented that Gerber formula is well suited to estimate the endurance limit of a DP590 sheet steel at different stress ratios for smooth specimen, while Goodman equation is more appropriate in the presence of stress concentration. Onn et al⁶¹ studied the effect of the mean stress on the HCF of a DP600 steel sheet. Walker's mean stress correction showed the best agreement with experimental data, while SWT, Goodman, and Morrow models needed an exponential calibration factor to obtain comparable results.

More recently, Walker model has been shown to well describe the mean stress effect of a stainless steel sheet, while other conventional equations were unreliable.⁶² Kujawski⁶³ proposed a modified SWT model to extend its accuracy to load ratios $R = \sigma_{min}/\sigma_{max} \leq -1$, for which it has been shown to be non-conservative.

3 | METHODS

3.1 | Material

A commercial grade DP600 steel produced by Salzgitter AG (Salzgitter, DE) was studied. The chemical composition is given in Table 1. The steel was supplied in a

TABLE 1 Chemical composition of the DP600 steel (wt%).

C	Si	Mn	P	S	N	Al	Cu	Cr	Ni	Mo	Nb	Ti	V
0.06	0.11	1.23	0.035	0.001	0.005	0.03	0.02	0.62	0.03	0.01	0.003	0.001	0.003

4.5 mm thick, 500 mm wide hot rolled sheet. The material was sampled from a unique coil.

3.2 | Experimental setup

Both static and fatigue (HCF and LCF) properties of the material were evaluated. Rolling direction was considered in the analysis; therefore, four combinations of

testing and pre-straining were studied, as shown in Figure 1A. First, uniform elongation values of the as-received condition of DP600 were obtained with tensile tests, in order to determine pre-strain levels (three uniformly spaced values up to necking of the material). The material was then cut into rectangular 130 × 500 mm sheets that were subjected to uni-axial pre-strain, and then specimens were obtained from the deformed plates.

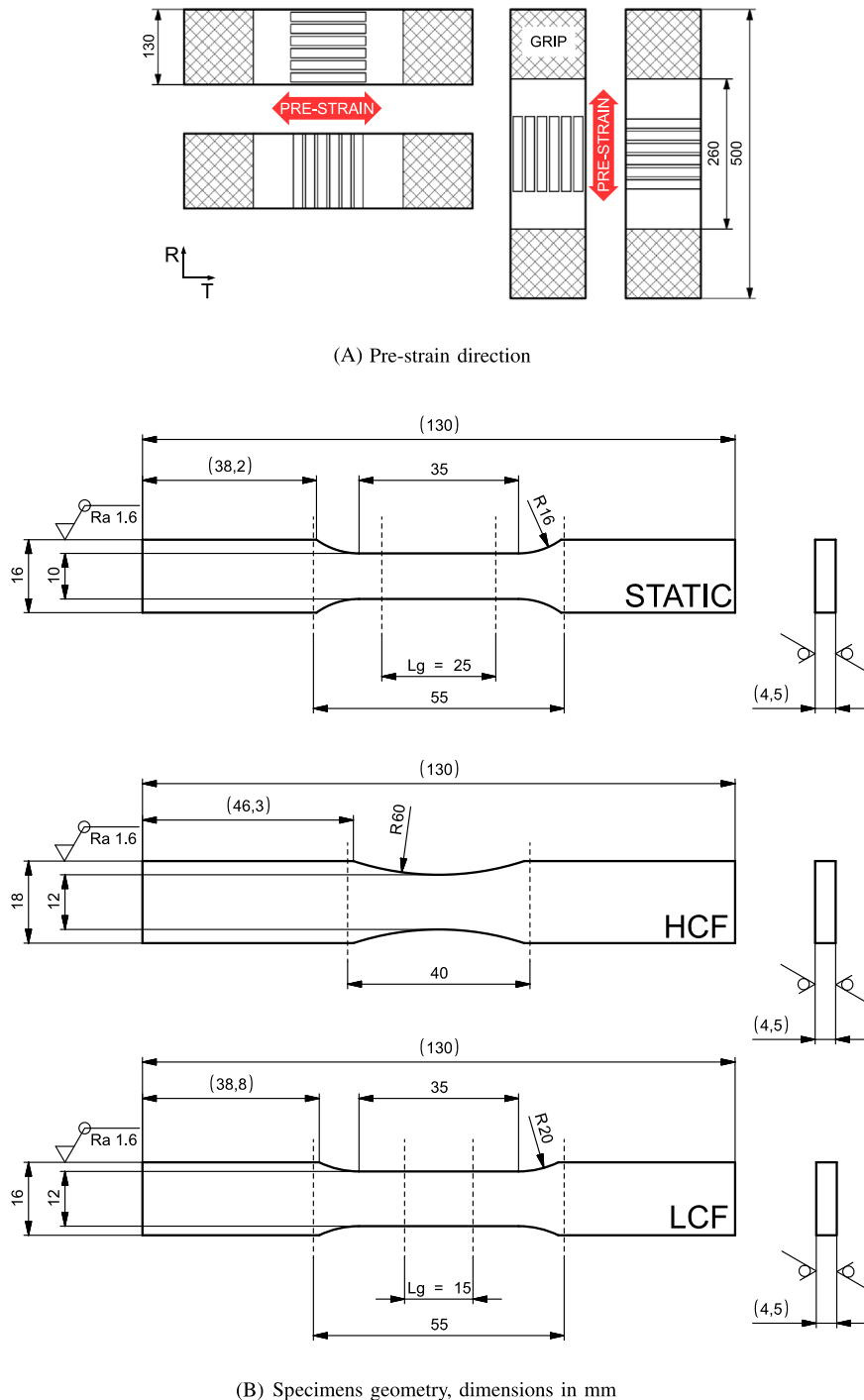


FIGURE 1 Experimental plan. [Colour figure can be viewed at wileyonlinelibrary.com]

Pre-strain of the rectangular specimen was applied using a Walter + Bai LFM 600 kN universal testing machine using custom made vices, strain control was performed using the built-in contact extensometer considering an initial gauge length of 100 mm and strain rate $\dot{\epsilon} = 0.002 \text{ s}^{-1}$. Pre-strain levels were checked using marks on the plates, and strain distribution was controlled using strain gauges on some of the samples. After pre-straining, specimens were cut from the deformed sheet via wire electrical discharge machining (WEDM), the final shape (Figure 1B) was then obtained by milling. The specimens geometries, for both static and fatigue tests, were slightly modified from the relevant ISO and ASTM standards^{64–69} for practical reasons (i.e., constrained maximum length of the specimen). Specimen surface was left unaltered from the original coil. Some specimens were then baked at 190° C for 35 min to reproduce the paint baking process.

Three levels of pre-strain were analyzed for static strength, three for HCF and two for LCF. All tests were conducted at room temperature of $23 \pm 2^\circ \text{ C}$.

Quasi-static tensile tests were performed using a Zwick Roell Z050 50 kN universal testing machine with a 50 kN load cell and contact extensometer. Fatigue strength characterization was carried out with a MTS Landmark 100 kN servo-hydraulic universal testing device.

Fully reversed ($R = \epsilon_{min}/\epsilon_{max} = -1$) low cycle fatigue tests were conducted under strain control with

triangular waveform using a clip-on extensometer, first load reversal being in tension. Frequencies were adapted to strain amplitude to maintain a constant strain rate $\dot{\epsilon} = 0.012 \text{ s}^{-1}$. To prevent buckling, a special device similar to that proposed by Xie et al⁷⁰ was applied to the specimens. This device is composed of two H-form steel brackets, which were fixed with screws on both sides of the specimen, as shown in Figure 2. A thin layer of PTFE was placed between the specimen and the steel brackets to reduce friction. Furthermore, small patches of epoxy resin were applied where the extensometer knife would contact the specimen to prevent slippage and surface damage.

Specimens were tested at three distinct levels of strain amplitude of $\Delta\epsilon/2 = 0.5\%$, 0.75% , and 1% . At least two specimens were tested for each strain amplitude and pre-strain condition. Total strain amplitude was considered for the fatigue model, as elastic deformation is assumed to be equal for the three levels:

$$\frac{\Delta\epsilon}{2} = \epsilon'_f N_f^c \quad (1)$$

High cycle fatigue tests were performed by stress controlled tests with $R = \sigma_{min}/\sigma_{max} = -1$ and $R = 0.05$ at 20 Hz frequency and sine waveform. At least two specimens were tested for each stress amplitude to generate



FIGURE 2 Setup for LCF tests. [Colour figure can be viewed at wileyonlinelibrary.com]

S-N curves. Run-out threshold was set to $2 \cdot 10^6$ cycles. HCF experimental data were fitted by least square to the Basquin model with N_f as dependent variable:

$$\frac{\Delta\sigma}{2} = \sigma'_f N_f^b \quad (2)$$

For both HCF and LCF, failure was defined as complete separation of the specimen in two parts.

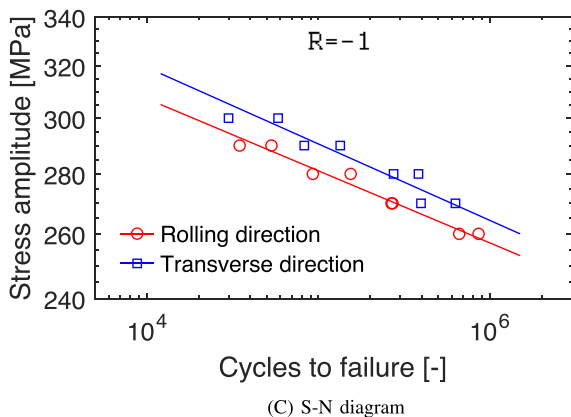
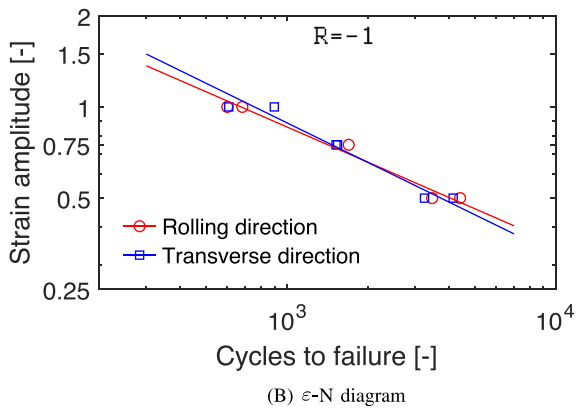
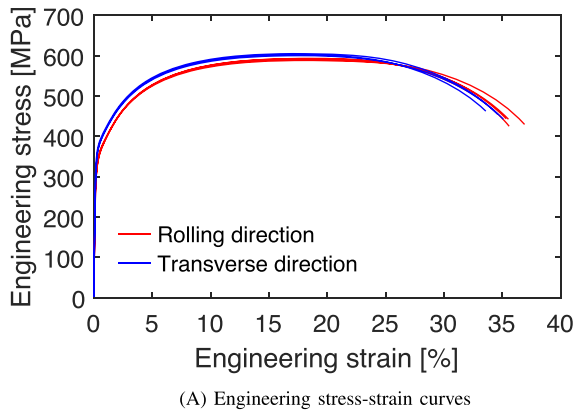


FIGURE 3 Properties of the as-received DP600 steel sheet. [Colour figure can be viewed at wileyonlinelibrary.com]

4 | RESULTS AND DISCUSSION

4.1 | As-received properties

4.1.1 | Tensile properties

As shown in Figure 3A, the material shows negligible anisotropy, with slightly higher strength and reduced ductility for transverse direction. The curves present continuous yielding without noticeable yield point and a

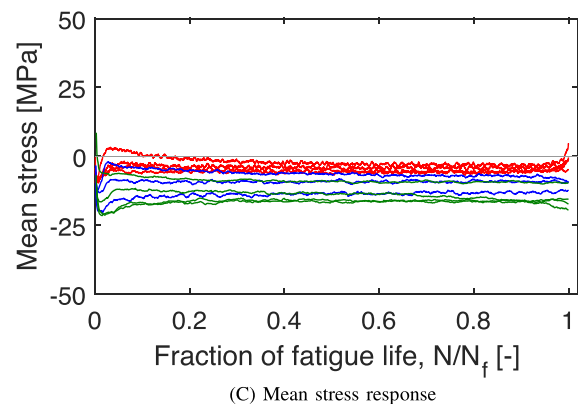
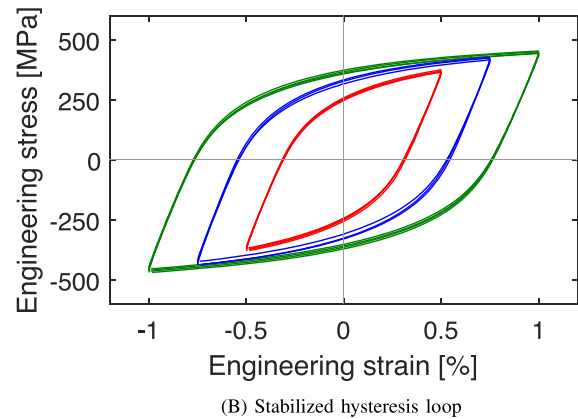
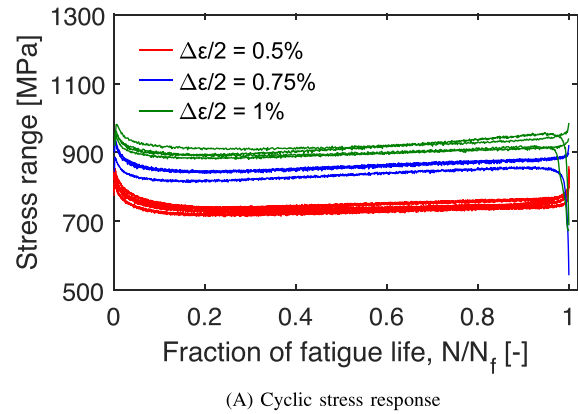


FIGURE 4 Cyclic response of the as-received DP600 steel sheet. [Colour figure can be viewed at wileyonlinelibrary.com]

prolonged plateau. Specimens revealed a typical ductile cup and cone fracture. Similar results are found in the literature for DP steels.^{9,28,29}

4.1.2 | Low-cycle fatigue

LCF experimental data, depicted in Figure 3B, has low scatter and exhibits insignificant anisotropy. A linear relationship between cycles to failure and strain amplitude seems to be adequate in the log-log plot. Model parameters are collected in Table A1.

Figure 4A shows the cyclic stress response of the DP600 sheet in its as-received condition. Softening is observed for the first couple of hundreds of cycles, and the response is fairly stable thereafter, with weak hardening. Increasing stress ranges in the last cycles before failure denote that the fractures occurred outside extensometer measurement span, which were mostly observed at the end of the parallel section of the specimen. These results were not excluded because values were in good agreement. Furthermore, since the majority of specimen failed near the fillet at the end of the parallel section, where a stress concentration is expected, data are supposed to be conservative.

Half-life stabilized hysteresis loops are shown in Figure 4B and indicate a very good repeatability of the LCF tests and confirm the isotropy observed in terms of short lives.

Figure 4C shows the mean stress of the hysteresis loop (computed as the difference between maximum and minimum value) for each cycle, which indicates the state of residual stresses in fully reversed strain tests. Compressive mean stress is observed for all strain amplitudes. This might be due to slightly higher friction with

the anti-buckling device during compression compared to tension³⁰ as a consequence of specimen expansion, which also explains why the measured mean stress tends to increase with strain amplitude. In fact, internal stresses can be reasonably considered negligible in as-received condition.

4.1.3 | High-cycle fatigue

Figure 3C shows HCF experimental data, which presents low scatter. Basquin equation fits the data well with the parameters collected in Table A1. In transverse direction, specimen exhibits superior fatigue resistance, probably due to the slightly higher strength observed in tensile tests,⁴⁰ but similar slope. Anyway, the material can reasonably be considered isotropic for practical purposes, with characterization in rolling direction representing a more conservative approach.

4.2 | Pre-strain

Following Figure 3A, three levels of pre-strain (i.e., 5%, 10%, and 15%) were chosen to characterize deformation up to necking.

4.3 | Effect of pre-strain

4.3.1 | Tensile properties

As expected, pre-strain increases strength and reduces ductility, as depicted in Figure 5. Higher levels of pre-strain lead to higher increment in strength and reduction of ductility. The increase in yield strength is due to higher

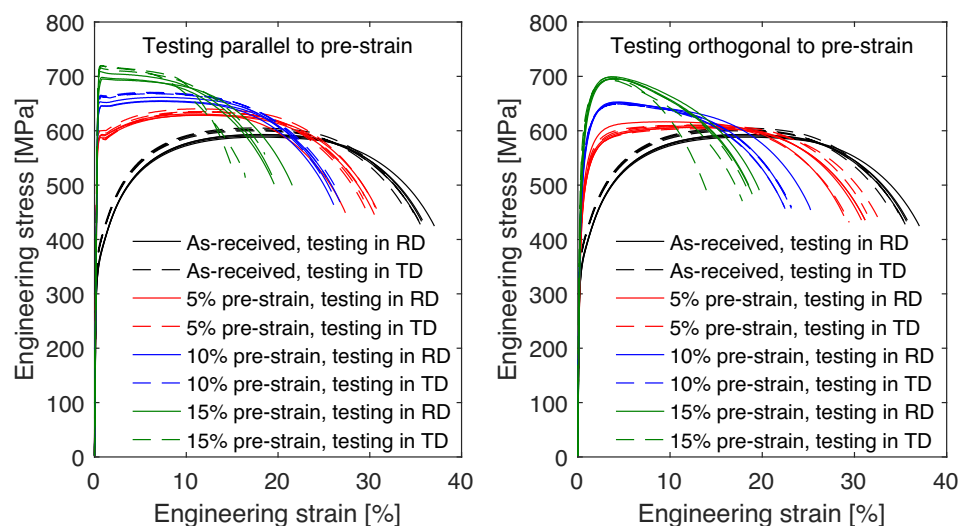


FIGURE 5 Engineering stress-strain curves of the as received DP600 and after pre-strain. [Colour figure can be viewed at wileyonlinelibrary.com]

dislocation density of the microstructure in pre-strained condition, which requires higher stress to be activated or reactivated during reloading.⁷¹ After pre-strain, anisotropy due to rolling direction tends to diminish, which is in contrast to what Das et al. observed for the same experiment set up on a DP600 steel.⁴⁰

Figure 6 plots strength and elongation against pre-strain level for both pre-strain conditions. Increase of ultimate tensile strength (UTS) and reduction in elongation follow a linear relationship and are little affected by pre-strain direction. Yield strength (0.2% offset) increment is well described with a power law:

$$\sigma_y = \sigma_y(0) + X\varepsilon_p^Y \quad (3)$$

With $\sigma_y(0) = 359$ MPa, $X = 122$ MPa, $Y = 0.383$ in the same direction as pre-strain and $\sigma_y(0) = 359$ MPa, $X = 38.3$ MPa, $Y = 0.610$ for orthogonal to pre-strain direction.

Furthermore, it was observed that change in strain path results in lower yield strength enhancement.

Figure 7 shows the true stress–strain curves of the as-received and pre-strained specimens. True stress and true strain are computed (up to UTS) as

$$\varepsilon_t = \ln(1 + \varepsilon) \quad (4)$$

$$\sigma_t = \sigma(1 + \varepsilon) \quad (5)$$

where ε and σ refer to the engineering values. In Figure 7, the flow curves are shifted on the strain axis to

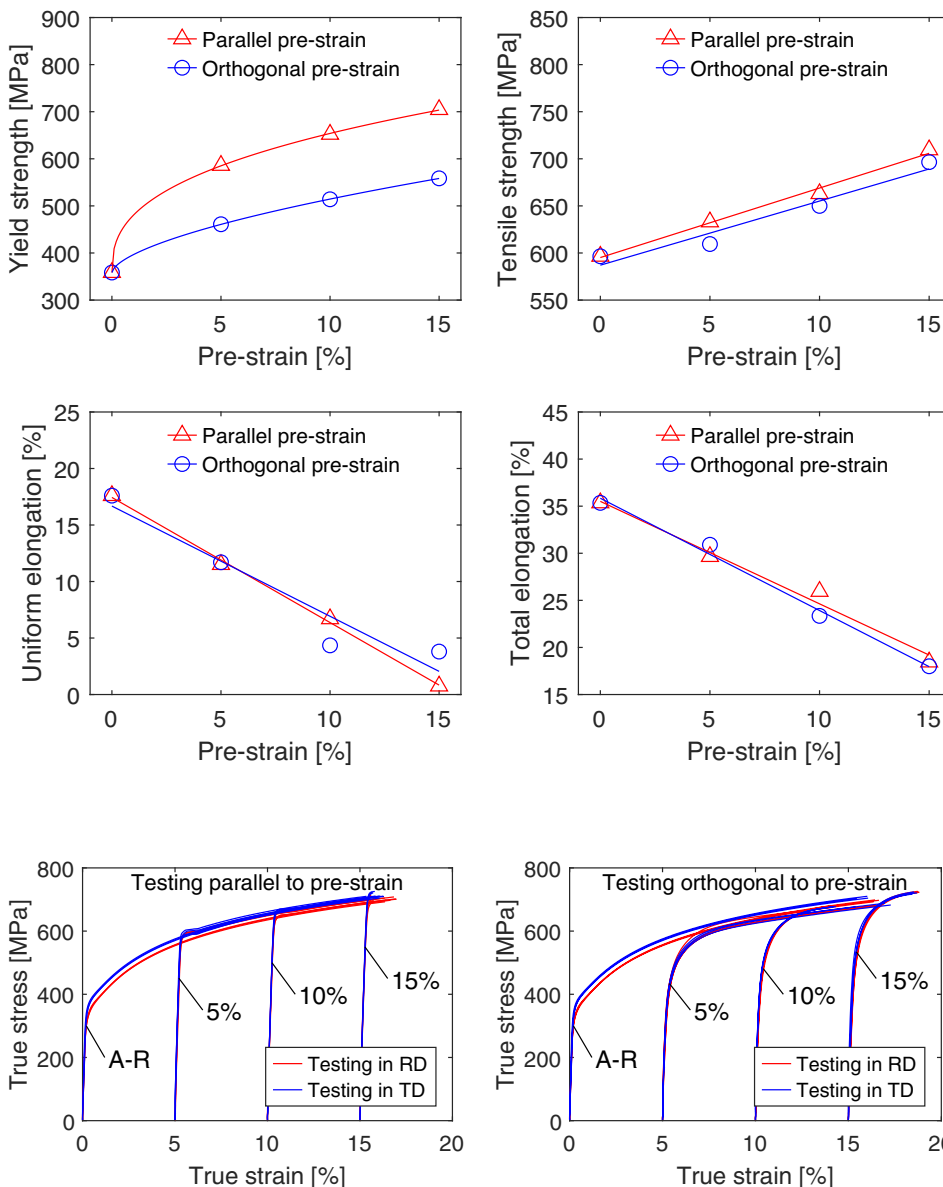


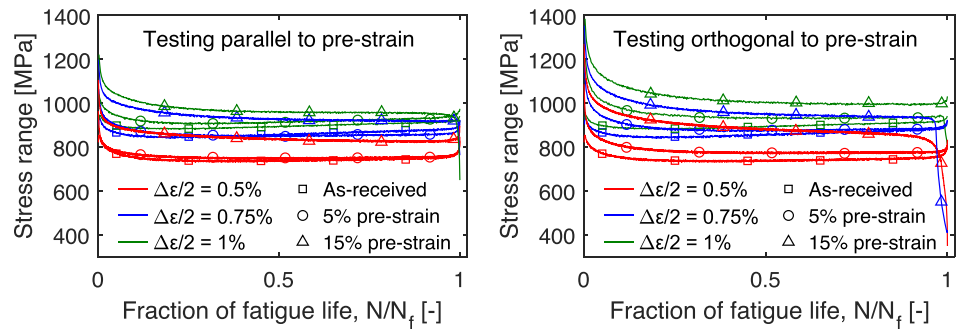
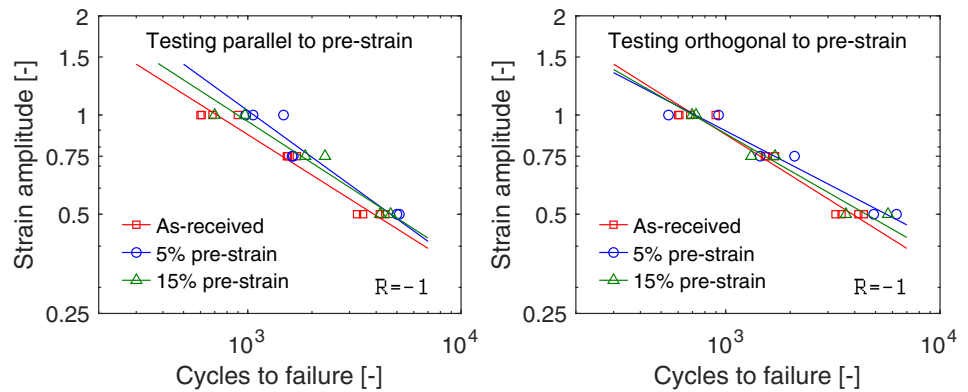
FIGURE 6 Evolution of some tensile properties after pre-strain (engineering values) [Colour figure can be viewed at wileyonlinelibrary.com]

FIGURE 7 True stress–strain curves of the as received DP600 and after pre-strain. [Colour figure can be viewed at wileyonlinelibrary.com]

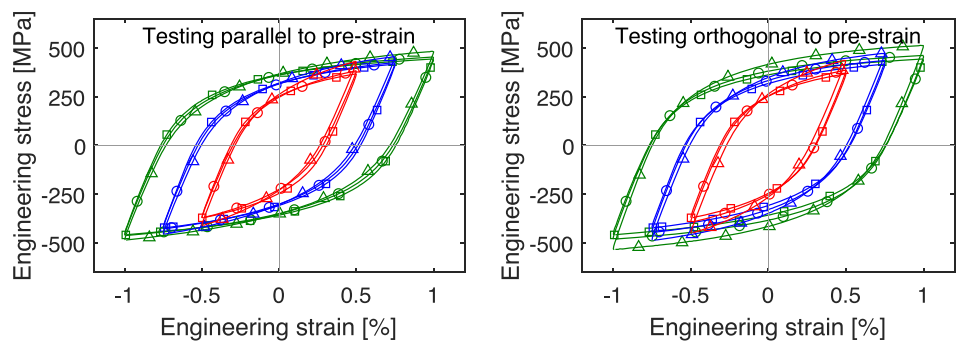
the nominal pre-strain level. After pre-strain and subsequent testing in the same direction, the behavior of the material follows that of the as received condition, with

increased and sharp yield point at stress values of the base curve for the same level of plastic strain. If the pre-strain is orthogonal to testing direction, yield strength

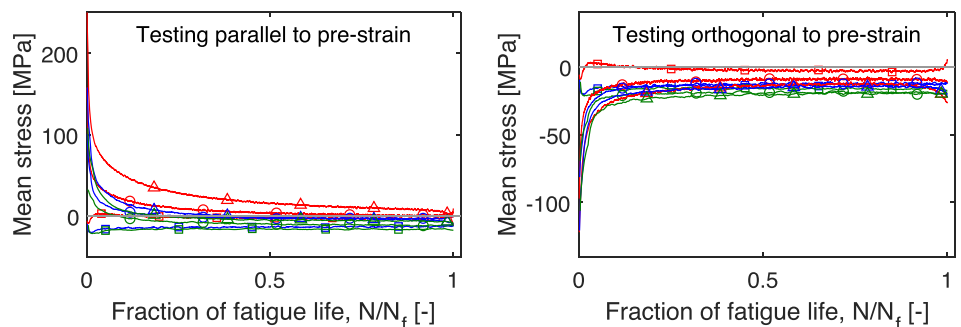
FIGURE 8 ϵ -N diagram of the as-received DP600 steel and after pre-strain. [Colour figure can be viewed at wileyonlinelibrary.com]



(A) Cyclic stress response



(B) Stabilized hysteresis loop



(C) Mean stress response

FIGURE 9 Cyclic response of the as-received and pre-strained DP600 steel. [Colour figure can be viewed at wileyonlinelibrary.com]

increases moderately and the flow curve exhibits continuous yielding. After a few percent plastic strain, however, the curves converge to the as-received condition.

These results confirm that strain path changes primarily affect elastic-plastic transition during early stages of reloading and strain path anisotropy is negligible at high level of reloading strain, as reported in previous studies.^{28,72} Similar behavior was observed in other studies.^{26,29,30,41} Different transient flow is attributed to residual stresses relaxation²⁸ while asymptotic response at high strains is caused by the progressive disruption or rearrangement of dislocation structures formed during latter deformation.⁷² Furthermore, other authors pointed out that a strain path change leads to different deformation zones (90° rotation) around hard martensite particles, which substantially modifies yielding behavior.⁴⁰

While small differences in tensile properties of the undeformed material due to rolling seem to be retained for specimens subjected to parallel pre-strain, this does not appear to be the case for orthogonal pre-strained specimens, where the anisotropy disappears. For this reason, rolling and transverse directions are not considered further to assess fatigue strength of the DP600 steel. In fact, the directions are often lost during industrial multi-step forming processes.

4.3.2 | Low-cycle fatigue

In Figure 8, for each pre-strain and strain amplitude level, a specimen for every combination illustrated by Figure 1 has been tested and grouped in two categories: testing parallel or orthogonal to pre-strain direction. Parameters for the Coffin-Manson model are collected in Table A1. No influence of prior deformation was found in LCF compared to HCF regimes. Results suggest that the effect on LCF is not proportional to pre-strain levels, as lives after 15% pre-strain fall between as-received and 5% pre-strain for both parallel and orthogonal testing for the strain amplitude analyzed. This could be due to the adversarial effect of increase in strength and decrease of ductility. A lower level of pre-strain might be favorable because it produces the best trade-off between the two phenomena.

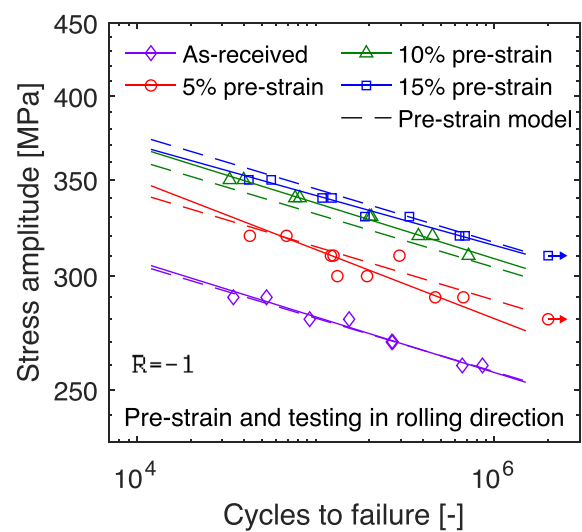
Negligible effect of pre-strain on LCF has been extensively reported in literature,^{21,34} but some authors observed a detrimental influence.³⁷

The cyclic response of DP600 after pre-strain is depicted in Figure 9A. For the sake of clarity, only one specimen is shown for each pre-strain condition and strain amplitude, as the behavior was practically identical in each setup. Furthermore, the behavior did not change

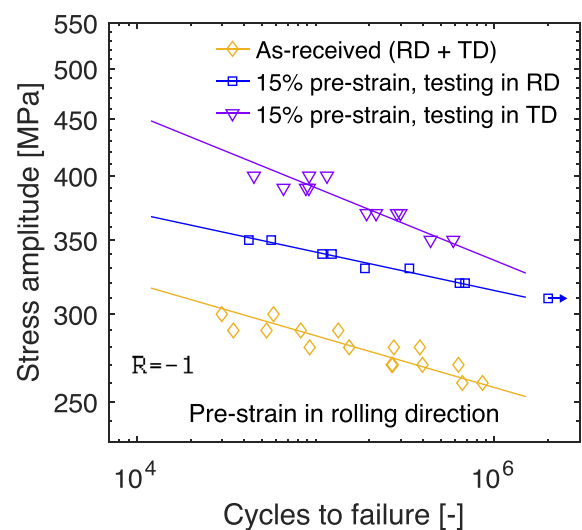
substantially after pre-strain, with softening occurring during the first hundreds of cycles.

Both cyclic hardening⁷³ and softening^{37,41,45} have been reported in literature for similar strength DP steels. Cycling softening is attributed to rearrangement of dislocation into low energy configurations, while cyclic hardening is caused by the increase of dislocation density.^{18,19,73}

At stabilized hysteresis loop (i.e., half number of cycles to failure), the material exhibited a close to unique flow curve after loading parallel to pre-strain direction, whereas small increases in flow stress were observed subsequently strain path change, especially for 15% pre-strain



(A) Effect of pre-strain level



(B) Effect of pre-strain direction

FIGURE 10 S-N diagrams of the as received and pre-strained DP600 steel sheet. [Colour figure can be viewed at wileyonlinelibrary.com]

(Figure 9B), which is contrary to monotonic results. The difference in stress amplitude is significantly smaller for the cyclic stress amplitude at stabilized loop than in monotonic testing. The effect of pre-strain is therefore largely lost due to softening in the first hundreds of cycles.

While the as-received material exhibits negligible mean stress throughout short life when subjected to fully reversed plastic deformation, after pre-strain mean stress is observed (Figure 9C). The residual stress is of tensile nature for parallel pre-strained specimens and compressive after orthogonal pre-strain and relaxes in the first hundreds of cycles. Magnitude of the mean stress increases with strain amplitude and pre-strain. Moreover, relaxation is faster at high strain amplitudes. At half-life, the residual stress is practically fully relaxed. These results find confirmation in previous studies.^{34,36,41}

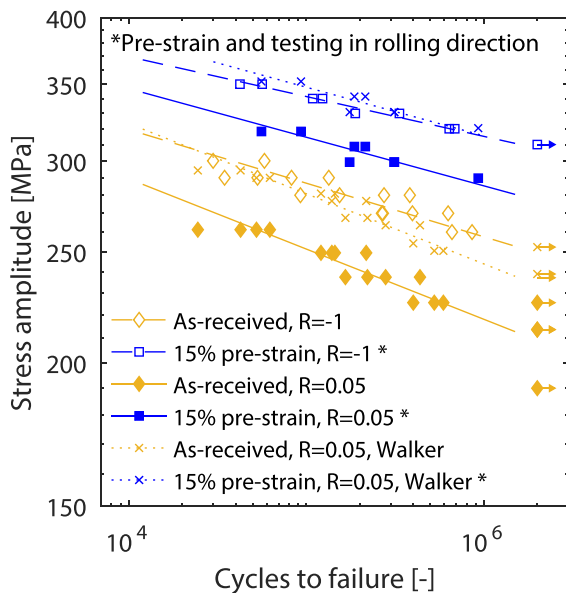


FIGURE 11 Comparison between S-N diagrams of the DP600 steel at different load ratios. [Colour figure can be viewed at [wileyonlinelibrary.com](https://onlinelibrary.wiley.com)]

From an empirical point of view, the mean stress response after pre-strain might be explained by the mixed kinematic and isotropic work hardening of DP steels observed in previous studies.^{30,74} Co-axial pre-strain and subsequent reloading are therefore characterized by Bauschinger effect (reduced yield strength in compression). The residual stress is therefore tensile in nature. Pre-strain causes compressive deformation in the direction perpendicular to tensile axis. Thereafter, due to Bauschinger effect, yield strength may be lower in tension, which explains why a compressive residual stress is observed after strain path change.

The aforementioned results indicate that the effect of pre-strain is lost under LCF life due to cyclic softening

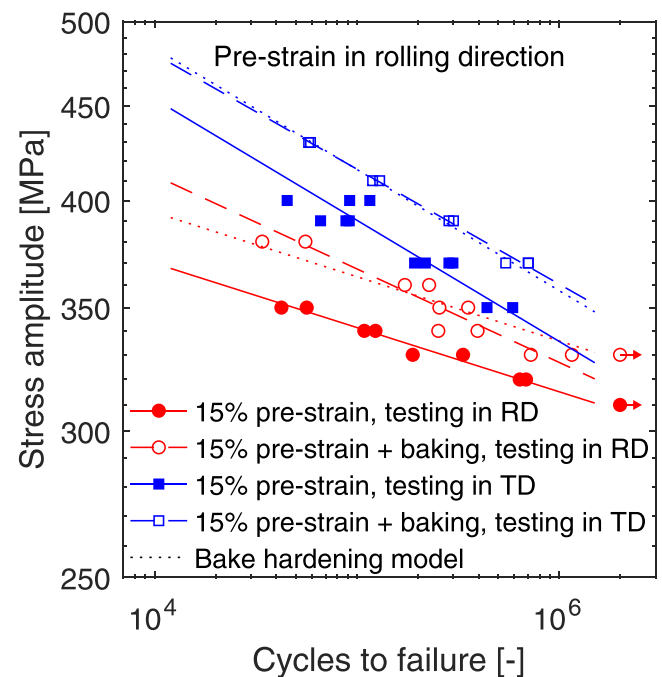
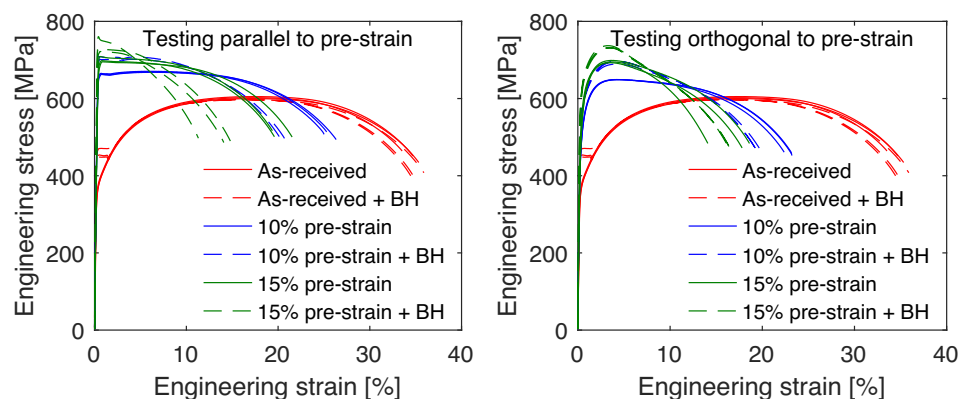


FIGURE 13 Comparison between S-N curves for the DP600 steel before and after baking at 190°C for 35 min. [Colour figure can be viewed at [wileyonlinelibrary.com](https://onlinelibrary.wiley.com)]

FIGURE 12 Engineering stress-strain curves of the as received DP600 and after pre-strain and baking. [Colour figure can be viewed at [wileyonlinelibrary.com](https://onlinelibrary.wiley.com)]



and residual stress relaxation, which explain the relatively small difference between the various conditions.

4.3.3 | High-cycle fatigue

A beneficial effect of pre-strain on HCF resistance was observed, as illustrated by Figure 10, with parameters for the stress life collected in Table A1.

The slope of the curve seems to be unaffected by pre-strain, while the fatigue strength increase is non proportional to pre-strain but tends to diminish with plastic deformation. Thus, a power law is used to describe the experimental data:

$$\frac{\Delta\sigma}{2} = (A + B\varepsilon_p^C)N_f^b \quad (6)$$

Fitting was performed in this case by means of mean square considering stress amplitude as the dependent variable. The proposed model is reasonably accurate with the parameters collected in Table A1, as depicted in Figure 10A with dashed curves.

At equivalent level of pre-strain, orthogonal reloading results in better fatigue strength (Figure 10B), which is in contrast with the lower increase in yield strength compared to orthogonal pre-strain. These results are however consistent to those of Das et al., who noticed a larger extension in HCF lives subsequently strain path change. This was attributed to the formation of compressive residual stresses around martensite particles in the direction perpendicular to tensile axis of pre-strain.⁴⁰ The same outcome was observed for biaxial pre-strain.⁴³ Therefore, only considering uniaxial pre-strain in the same direction as testing is a conservative approach for fatigue life assessment.

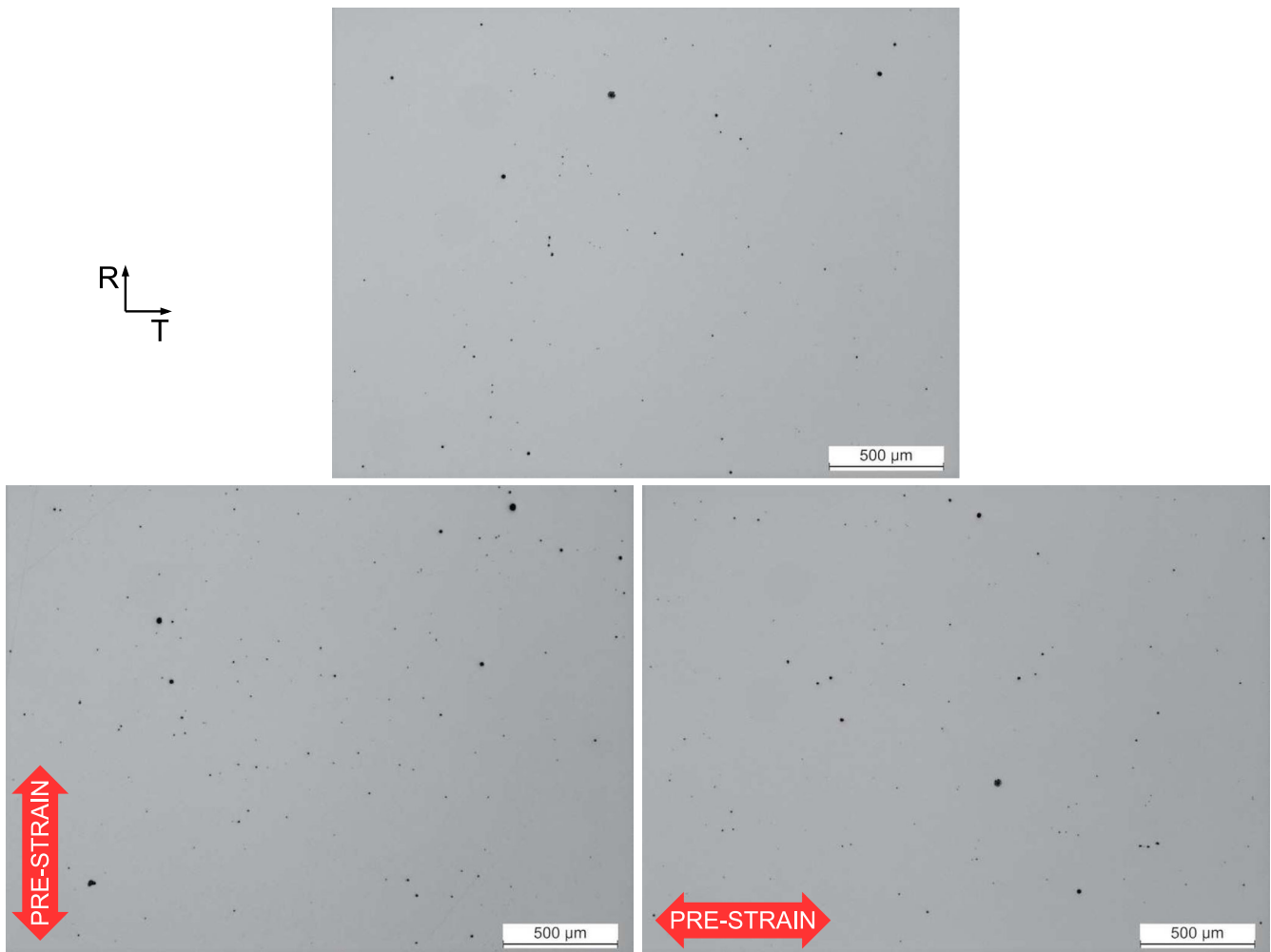


FIGURE 14 Optical microscopy of the DP600 before etching in both as received and pre-strained conditions. [Colour figure can be viewed at wileyonlinelibrary.com]

4.3.4 | Mean stress effect

There is a strong detrimental effect of a positive mean stress compared to fully reversed loading, as shown in Figure 11. Stress amplitude values of tests performed at $R = 0.05$ have been transformed to equivalent levels at $R = -1$ using Walker equation:

$$\sigma_{eq} = \sigma \left(\frac{2}{1-R} \right)^{1-\gamma} \quad (7)$$

with $\gamma = 0.85$. Walker mean stress correction shows good agreement with experimental data in both as received and pre-strained conditions.

4.4 | Effect of bake hardening

4.4.1 | Tensile properties

Bake hardening further increases the strength as shown in Figure 12. For the as-received condition, the difference

only affects the first stage of the deformation and the flow curves converge thereafter. Furthermore, it is observed that bake hardening slightly reduces ductility, especially after pre-strain.

4.4.2 | High-cycle fatigue

The effect of bake hardening on HCF is depicted in Figure 13, with parameters of the curves in Table A1. The slope of the curve is not much affected after the baking process, but the fatigue resistance is highly increased. In consideration of these results, a multiplier for the fatigue strength coefficient is proposed as a correction factor to take into account the bake hardening effect in HCF:

$$\frac{\Delta \varepsilon}{2} = \alpha_{BH} \sigma'_f (2N)^b \quad (8)$$

with $\alpha_{BH} = 1.065$ fitting both curves well ($R^2 = 0.85$ and $R^2 = 0.99$ for rolling and transverse direction, respectively).

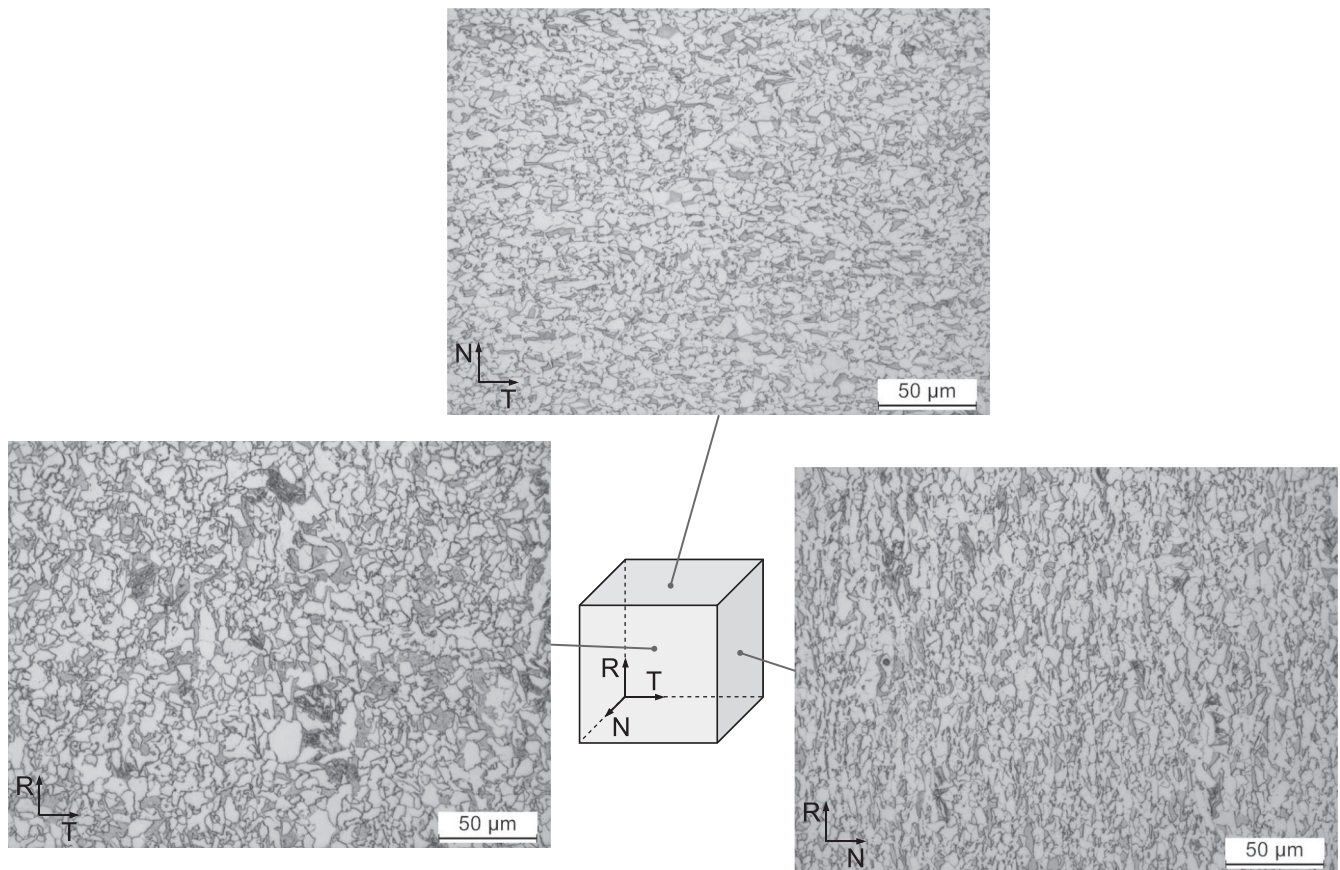


FIGURE 15 Optical microscopy of the as-received material.

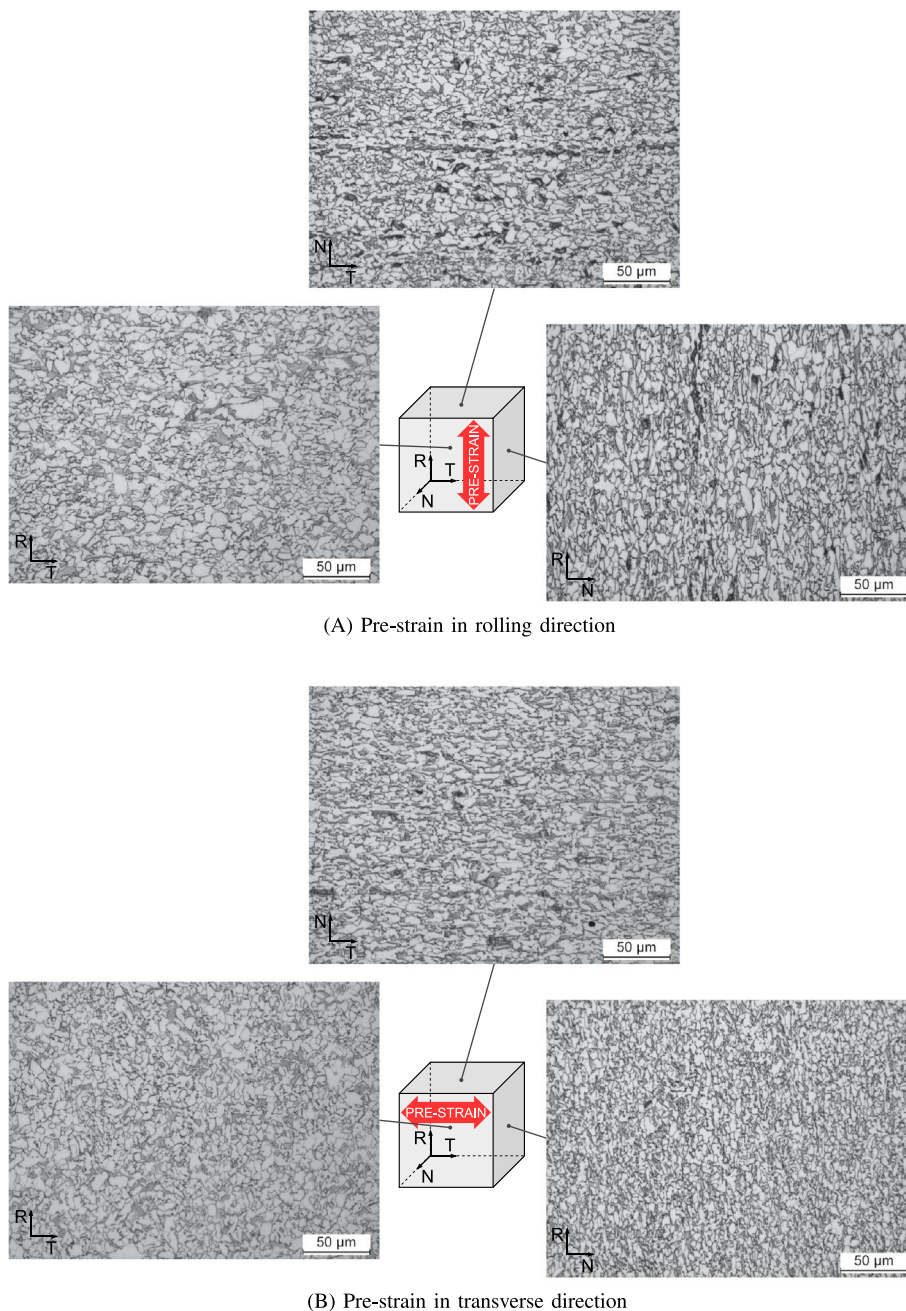
4.5 | Microstructure analysis

As-received and 15% pre-strained in rolling and transverse direction specimens were cut along the three principal planes, mirror polished and etched using a 2% nital solution.

Uniformly distributed spherical voids were observed in both as-received and pre-strained material (Figure 14). Average porosity of 0.1% was evaluated on 10 samples using ImageJ software. Pre-strain did not change noticeably voids shape or distribution. Similar remarks were not found in literature. Nevertheless, fatigue cracks nucleate from the surface of the specimens, which indicates that porosity does not influence early stages of fatigue.

The microstructure of the as-received DP600 steel is composed of ferrite and martensite, as shown in Figure 15. There is not a noticeable difference between rolling and transverse direction, but grains are flattened in thickness direction (N) as a consequence of the rolling process. The negligible microstructure anisotropy of the as-received material is reflected in tensile properties.

The behavior of the material cannot be explained in terms of microstructure texture evolution as no significant difference is observed after pre-strain,²⁶ as shown in Figure 16. However, appreciable changes in microstructure have also been reported in literature.^{37,75}



(A) Pre-strain in rolling direction

(B) Pre-strain in transverse direction

FIGURE 16 Optical microscopy of the material subjected to 15% pre-strain. [Colour figure can be viewed at wileyonlinelibrary.com]

5 | CONCLUSION

The present work consists of static and fatigue properties assessments of a DP600 steel sheet in as-received and uni-axial tensile pre-strained conditions. The material was subjected to different strain paths, namely, testing was performed in the same direction or 90° to pre-strain. Tensile, stress controlled, and fully reversed strain controlled tests were performed for each strain path combination. Furthermore, the effect of the paint baking process on the static and high cycle fatigue strength of the DP600 sheet was studied. The following conclusion were drawn from the experimental results:

- The material, in both as-received and pre-strained condition, exhibited negligible anisotropy from the rolling process.
- Pre-strain increased yield and tensile strength and reduced ductility regardless of pre-straining method due to work hardening. Flow curves manifested sharp yielding during reloading in the same direction as pre-strain, whereas lower and continuous yield was observed after orthogonal pre-strain, but the behavior converges after few percent subsequent plastic deformation. The material substantially follows as-received behavior in term of true stress-strain, considering strain accumulation. A power-law increase of yield strength was observed after pre-strain, while ultimate tensile strength increases linearly.
- High increase in high cycle fatigue resistance was observed after pre-strain, and this improvement was attributed primarily due to yield strength enhancement. Testing along the tensile axis of previous deformation results however in slightly worse fatigue resistance compared to the orthogonal direction.
- A model with a pre-strain dependent fatigue strength coefficient was proposed for HCF assessment and was in good agreement with the experimental data.
- Stress controlled tests with load ratio $R = 0.05$ revealed that tensile mean stress is highly detrimental for fatigue. Experimental data correlates well with Walker mean stress correction model.
- Bake hardening was observed to influence the behavior of the tensile properties only near yield for the as received condition, while the strength is enhanced throughout the flow curve for pre-strained material. This results in improved fatigue strength, which can be assessed adding a constant to the fatigue strength coefficient.
- Material exhibited negligible mean stress in as-received condition during fully reversed strain tests. Orthogonal pre-strain introduced a compressive residual stress, as opposed to the tensile value when testing parallel to the pre-strain direction. The development of the

residual stress was qualitatively explained by the Bauschinger effect. However, the effect of pre-strain is gradually lost during LCF life due to cyclic softening and residual stress relaxation, which results in weak influence of prior deformation in low cycle fatigue, regardless of strain path.

- The monotonic and cyclic quasi-isotropic properties of the DP600 can be attributed to the uniform microstructure of the steel in rolling and transverse direction, as revealed by the optical microscopy, but the effect of pre-straining cannot be explained by texture evolution.

AUTHOR CONTRIBUTIONS

Andrea Kusch: Methodology; formal analysis; visualization; writing—original draft. **Daniele Crivelli:** Funding acquisition; project administration; investigation. **Luca Diviani:** Conceptualization; funding acquisition; review. **Matteo Dotta:** Investigation. **Simone Salamina:** Methodology; investigation; formal analysis. **Filippo Berto:** Methodology; review.

ACKNOWLEDGMENTS

The authors would like to thank Alcar Ruote SA (Manno, CH) for providing the material, supporting the research in this study and giving permission to publish this article. Open access funding provided by Scuola Universitaria Professionale della Svizzera Italiana.

CONFLICT OF INTEREST STATEMENT

The authors declare that they have no known competing financial interests or personal relationships that could have appeared to influence the work reported in this paper.

DATA AVAILABILITY STATEMENT

The data that support the findings of this study are available upon reasonable request.

ORCID

Filippo Berto  <https://orcid.org/0000-0001-9676-9970>

REFERENCES

1. Shang D, Liu X, Shan Y, Jiang E. Research on the stamping residual stress of steel wheel disc and its effect on the fatigue life of wheel. *Int J Fatigue*. 2016;93:173-183.
2. Meng J, Zhu P, Liu Z, Ji Q. Integration of multi-step stamping effects in the bending fatigue analysis of a steel wheel. *Fatigue Fract Eng Mater Struct*. 2013;36(8):795-808.
3. Wang X, Zhang X. Simulation of dynamic cornering fatigue test of a steel passenger car wheel. *Int J Fatigue*. 2010;32(2):434-442.
4. Fonstein N. 7 - Dual-phase steels. In: Rana R, Singh SB, eds. *Automotive Steels*: Woodhead Publishing; 2017:169-216.
5. Atreya V, Bos C, Santofimia MJ. Understanding ferrite deformation caused by austenite to martensite transformation in dual phase steels. *Scripta Mater*. 2021;202:114032.

6. Sarwar M, Priestner R. Influence of ferrite-martensite microstructural morphology on tensile properties of dual-phase steel. *J Mater Sci*. 1996;31(8):2091-2095. <https://doi.org/10.1007/BF00356631>
7. Badkoobeh F, Mostaan H, Rafiei M, Bakhsheshi-Rad HR, Berto F. Microstructural characteristics and strengthening mechanisms of ferritic–martensitic dual-phase steels: a review. *Metals*. 2022;12(1):101.
8. Ghadbeigi H, Pinna C, Celotto S, Yates JR. Local plastic strain evolution in a high strength dual-phase steel. *Mat Sci Eng A-struct*. 2010;527(18):5026-5032.
9. Kadkhodapour J, Butz A, Ziaei Rad S. Mechanisms of void formation during tensile testing in a commercial, dual-phase steel. *Acta Mater*. 2011;59(7):2575-2588.
10. Davies RG. Influence of martensite composition and content on the properties of dual phase steels. *Metall Trans A*. 1978;9(5):671-679. <https://doi.org/10.1007/BF02659924>
11. Mediratta SR, Ramaswamy V, Rao PR. Influence of ferrite-martensite microstructural morphology on the low cycle fatigue of a dual-phase steel. *Int J Fatigue*. 1985;7(2):107-115.
12. Sherman AM, Davies RG. The effect of martensite content on the fatigue of a dual-phase steel. *Int J Fatigue*. 1981;3(1):36-40.
13. Sherman AM, Davies RG. Influence of martensite carbon content on the cyclic properties of dual-phase steel. *Int J Fatigue*. 1981;3(4):195-198.
14. Park K, Nishiyama M, Nakada N, Tsuchiyama T, Takaki S. Effect of the martensite distribution on the strain hardening and ductile fracture behaviors in dual-phase steel. *Mat Sci Eng A-struct*. 2014;604:135-141.
15. Sun Z, Wang Z, Ai S. Effects of morphology on the tensile and fatigue behaviour of a dual-phase steel. *Steel Res*. 1989;60(5):215-220. <https://doi.org/10.1002/srin.198900277>
16. Wang ZG, Ai SH. Fatigue of martensite-ferrite high strength low-alloy dual phase steels. *Isij Int*. 1999;39(8):747-759.
17. Sarwar M, Priestner R, Ahmad E. Influence of martensite volume fraction on fatigue limit of a dual-phase steel. *J Mater Eng Perform*. 2002;11(3):274-277. <https://doi.org/10.1361/105994902770344060>
18. Paul SK, Stanford N, Hilditch T. Effect of martensite volume fraction on low cycle fatigue behaviour of dual phase steels: Experimental and microstructural investigation. *Mat Sci Eng A-struct*. 2015;638:296-304.
19. Zhongguang W, Guonan W, Wei K, Haicai H. Influence of the martensite content on the fatigue behaviour of a dual-phase steel. *Mater Sci Eng*. 1987;91:39-44.
20. Paul SK, Stanford N, Hilditch T. Effect of martensite morphology on low cycle fatigue behaviour of dual phase steels: experimental and microstructural investigation. *Mat Sci Eng A-struct*. 2015;644:53-60.
21. Fredriksson K, Melander A, Hedman M. Influence of prestraining and ageing on fatigue properties of high-strength sheet steels. *Int J Fatigue*. 1988;10(3):139-151.
22. Fredriksson K, Melander A, Hedman M. Influence of prestraining and ageing on the fatigue properties of a dual phase sheet steel with tensile strength of 410 MPa. *Scand J Metall*. 1989;18(4):155-165.
23. Hill SI, Kuhlman SH, Wang K, Belwafa J, Chen X. Bake-Hardening Effect of Dual Phase Steels. *Technical report*, Warrendale, PA; 2009.
24. Le Q, Kang H, Khosrovaneh A, Sa CY, Yan B. Prestrain Effect on Fatigue of DP600 Sheet Steel. *Technical report*, SAE Technical Paper; 2007.
25. Sherman AM. Fatigue properties of high strength-low alloy steels. *Metall Trans A*. 1975;6(5):1035. <https://doi.org/10.1007/BF02661357>
26. Liao J, Sousa JA, Lopes AB, Xue X, Barlat F, Pereira AB. Mechanical, microstructural behaviour and modelling of dual phase steels under complex deformation paths. *Int J Plast*. 2017;93:269-290.
27. Pascoe KJ. Directional effects of prestrain in steel. *J Strain Anal*. 1971;6(3):181-184.
28. Tarigopula V, Hopperstad OS, Langseth M, Clausen AH. Elastic-plastic behaviour of dual-phase, high-strength steel under strain-path changes. *Eur J Mech A Solids*. 2008;27(5):764-782.
29. Yu HY, Shen JY. Evolution of mechanical properties for a dual-phase steel subjected to different loading paths. *Mater Design*. 2014;63:412-418.
30. Sun L, Wagoner RH. Proportional and non-proportional hardening behavior of dual-phase steels. *Int J Plasticity*. 2013;45:174-187.
31. Kim H, Kim C, Barlat F, Pavlina E, Lee MG. Nonlinear elastic behaviors of low and high strength steels in unloading and reloading. *Mat Sci Eng A-struct*. 2013;562:161-171.
32. Zhao Y, Ma M, Qin R, Ling Y, Wang G, Wan X, Gu H, Liu Y. A fabrication history based strain-fatigue model for prediction of crack initiation in a radial loading wheel. *Fatigue Fract Eng Mater Struct*. 2017;40(11):1882-1892.
33. Gustavsson A, Larsson M, Melander A. Fatigue life of pressed steel sheet components. *Int J Fatigue*. 1997;19(8-9):613-619.
34. Gustavsson A, Melander A. Fatigue of a highly prestrained dual-phase sheet steel. *Fatigue Fract Eng Mater Struct*. 1995;18(2):201-210. <https://doi.org/10.1111/j.1460-2695.1995.tb00155.x>
35. Sherman AM, Davies RG. Fatigue of a dual-phase steel. *Metall Trans A*. 1979;10(7):929-933.
36. Gustavsson A, Melander A. Variable-amplitude fatigue of a dual-phase sheet steel subjected to prestrain. *Int J Fatigue*. 1994;16(7):503-509.
37. Le Q, Kang HT, Kridli G, Khosrovaneh AK, Yan B. Effect of prestrain paths on mechanical behavior of dual phase sheet steel. *Int J Fatigue*. 2009;31(4):607-615.
38. Le Q, Kang H, Kridli G, Khosrovaneh A, Yan B. Modified strain-life equation to consider the effect of different prestrain paths for dual phase sheet steel. *J Mater Process Tech*. 2009;209(7):3525-3531.
39. Das B, Paul SK, Singh A, Arora KS, Shome M. The effect of thickness variation and pre-strain on the cornering fatigue life prediction of a DP600 steel wheel disc. *Int J Fatigue*. 2020;139:105799.
40. Das B, Singh A, Arora KS, Shome M, Paul SK. Influence of prestraining path on high cycle fatigue performance of DP 600 steel. *Int J Fatigue*. 2019;126:369-380.
41. Das B, Singh A, Paul SK. Low cycle fatigue performance of DP600 steel under various pre-straining paths. *Int J Fatigue*. 2020;132:105331.
42. Ghosal P, Paul SK, Das B, Chinara M, Arora KS. Notch fatigue performance of DP600 steel under different pre-straining paths. *Theor Appl Fract Mec*. 2020;108:102630.

43. Ghosal P, Paul SK, Raj A. Influence of uniaxial and biaxial pre-straining on the high cycle fatigue performance of DP590 steel. *Int J Fatigue*. 2021;151:106369.
44. Ghosal P, Paul SK, Raj A. Influence of uniaxial and biaxial pre-straining on the notch fatigue performance of DP590 steel. *Theor Appl Fract Mec*. 2021;115:103072.
45. Ghosal P, Raj A, Paul SK. Influence of uniaxial and biaxial pre-straining on the low cycle fatigue performance of DP590 steel. *Int J Fatigue*. 2021;149:106260.
46. Louge J, Moyne S, Doudard C, Calloch S, Weber B, Munier R. Self-heating measurements under cyclic loading to identify history effects on HCF properties of high-strength low-alloy steel: Part II – Modeling. *Fatigue Fract Eng Mater Struct*. 2022;45(12):3524-3534.
47. Louge J, Moyne S, Doudard C, Calloch S, Weber B, Munier R. Self-heating measurements under cyclic loading to identify history effects on HCF properties of high-strength low-alloy steel: Part I—experimental investigations. *Fatigue Fract Eng Mater Struct*. 2023;46(1):171-181.
48. Paul SK. Effect of forming strain on low cycle, high cycle and notch fatigue performance of automotive grade dual phase steels: a review. *Forces Mech*. 2023;11:100184.
49. Kuang CF, Zhang SG, Li J, Wang J, Liu HF. Effects of pre-strain and baking parameters on the microstructure and bake-hardening behavior of dual-phase steel. *Int J Miner Metall Mater*. 2014;21(8):766-771. <https://doi.org/10.1007/s12613-014-0969-7>
50. Pereloma E, Timokhina I. 9 - Bake hardening of automotive steels. In: Rana R, Singh SB, eds. *Automotive Steels*: Woodhead Publishing; 2017:259-288.
51. Ramazani A, Bruehl S, Abbasi M, Bleck W, Prah U. The effect of bake-hardening parameters on the mechanical properties of dual-phase steels. *Steel Res Int*. 2016;87(11):1559-1565. <https://doi.org/10.1002/srin.201600060>
52. Ramazani A, Bruehl S, Gerber T, Bleck W, Prah U. Quantification of bake hardening effect in DP600 and TRIP700 steels. *Mater Design*. 2014;57:479-486.
53. Tosal-Martnez L, Keichel J, Akdut N. Fatigue behavior of multiphase steels for automotive applications. In: Proceedings of the 10th International Congress on Fracture. Citeseer; 2001.
54. Wasn J, Karlsson B. Influence of prestrain and ageing on near-threshold fatigue crack growth in fine-grained dual-phase steels. *Int J Fatigue*. 1989;11(6):395-405.
55. Sperle JO. Fatigue strength of high strength dual-phase steel sheet. *Int J Fatigue*. 1985;7(2):79-86.
56. Gündüz S. Static strain ageing behaviour of dual phase steels. *Mat Sci Eng A-struct*. 2008;486(1):63-71.
57. Ji D, Zhang M, Zhu D, Luo S, Li L. Influence of microstructure and pre-straining on the bake hardening response for ferrite-martensite dual-phase steels of different grades. *Mat Sci Eng A-struct*. 2017;708:129-141.
58. Lee YL, Barkey ME, Kang HT. *Metal Fatigue Analysis Handbook: Practical Problem-Solving Techniques for Computer-Aided Engineering*: Elsevier; 2011. <https://www.sciencedirect.com/book/9780123852045/metal-fatigue-analysis-handbook>
59. Dowling NE, Calhoun CA, Arcari A. Mean stress effects in stress-life fatigue and the Walker equation. *Fatigue Fract Eng Mater Struct*. 2009;32(3):163-179.
60. Giri SK, Bhattacharjee D. Fatigue behavior of thin sheets of DP590 dual-phase steel. *J Mater Eng Perform*. 2012;21(6):988-994. <https://doi.org/10.1007/s11665-011-9992-2>
61. Onn IH, Ahmad N, Tamin MN. Fatigue characteristics of dual-phase steel sheets. *J Mech Sci Technol*. 2015;29(1):51-57.
62. Oh G. Effective stress and fatigue life prediction with mean stress correction models on a ferritic stainless steel sheet. *Int J Fatigue*. 2022;157:106707.
63. Kujawski D. An interpretation and modification of the SWT function. *Fatigue Fract Eng Mater Struct*. 2021;44(8):2202-2209.
64. ASTM E466 - 21. Standard Practice for Conducting Force Controlled Constant Amplitude Axial Fatigue Tests of Metallic Materials. *Standard*, West Conshohocken, USA, American Society for Testing and Materials International. <https://www.astm.org/standards/e466>
65. ASTM E606 / E606M - 21. Standard Test Method for Strain-Controlled Fatigue Testing. *Standard*, West Conshohocken, USA, American Society for Testing and Materials International. https://www.astm.org/e0606_e0606m-21.html
66. ASTM E8 / E8M - 21. Standard Test Methods for Tension Testing of Metallic Materials. *Standard*, West Conshohocken, USA, American Society for Testing and Materials International. https://www.astm.org/e0008_e0008m-21.html
67. ISO 1099:2017. Metallic Materials—Fatigue—Testing Axial Force-Controlled Method. *Standard*, Geneva, CH, International Organization for Standardization. <https://www.iso.org/standard/67847.html>
68. ISO 12106:2017. Metallic Materials—Fatigue Testing—Axial-Strain-Controlled Method. *Standard*, Geneva, CH, International Organization for Standardization. <https://www.iso.org/standard/64687.html>
69. ISO 6892-1:2019. Metallic Materials—Tensile Testing—Part 1: Method of Test at Room Temperature. *Standard*, Geneva, CH, International Organization for Standardization. <https://www.iso.org/standard/78322.html>
70. Xie Z, Chen Y. Experimental and modeling study of cyclic plasticity and ductile fracture of thin structural steel sheets. *Thin Wall Struct*. 2021;162:107658.
71. Yan B, Belanger P, Citrin K. Effect of forming strain on fatigue performance of a mild automotive steel. *SAE Trans*. 2001;110:62-71.
72. Gardey B, Bouvier S, Richard V, Bacroix B. Texture and dislocation structures observation in a dual-phase steel under strain-path changes at large deformation. *Mat Sci Eng A-struct*. 2005;400-401:136-141.
73. Hadianfard MJ. Low cycle fatigue behavior and failure mechanism of a dual-phase steel. *Mat Sci Eng A-struct*. 2009;499(1):493-499.
74. Weiss M, Kupke A, Manach PY, Galdos L, Hodgson PD. On the Bauschinger effect in dual phase steel at high levels of strain. *Mat Sci Eng A-struct*. 2015;643:127-136.
75. Hosseini-Toudeshky H, Anbarlooie B, Kadkhodapour J, Shadalooyi G. Microstructural deformation pattern and mechanical behavior analyses of DP600 dual phase steel. *Mat Sci Eng A-struct*. 2014;600:108-121.

How to cite this article: Kusch A, Crivelli D, Diviani L, Dotta M, Salamina S, Berto F. Influence of pre-strain and bake hardening on the static and fatigue strength of a DP600 steel sheet. *Fatigue Fract Eng Mater Struct*. 2023;1-18. doi:10.1111/ffe.14095

APPENDIX A: PARAMETERS ESTIMATES
TABLE A1 Parameters for fatigue models.

As-received									
LCF					HCF				
Testing	ϵ'_f	c	R^2		Testing	σ'_f	b	R^2	
RD	12.36	-0.386	0.98		RD	438	-0.0387	0.97	
TD	17.75	-0.434	0.94		TD	466	-0.0410	0.91	
RD + TD	14.68	-0.409	0.96		RD + TD	492	-0.0468	0.82	
Pre-strained									
LCF					HCF				
Pre-strain	Testing	ϵ'_f	c	R^2	Pre-strain	Testing	σ'_f	b	R^2
5% RD + TD	RD + TD	26.32	-0.469	0.93	5% RD	RD	545	-0.0481	0.77
5% RD + TD	TD + RD	9.23	-0.338	0.90	10% RD	RD	527	-0.0388	0.99
15% RD + TD	RD + TD	17.27	-0.420	0.95	15% RD	RD	510	-0.0348	0.97
15% RD + TD	TD + RD	11.51	-0.373	0.95	15% RD	TD	831	-0.0656	0.87
Pre-strained and baked									
HCF									
Pre-strain	Testing			σ'_f		b		R^2	
15% RD	RD			658		-0.0506		0.90	
15% RD	TD			831		-0.0656		0.99	
Mean stress									
HCF									
Load ratio	Pre-strain	Testing		σ'_f		b		R^2	
0.05	As-received	RD+TD		508		-0.0613		0.86	
0.05	15% RD	RD		512		-0.0424		0.85	
Modified Basquin equation									
A	B	C		b		R^2			
431	299	0.582		-0.0373		0.97			